Study of multiband disordered systems using the typical medium dynamical cluster approximation

Yi Zhang,[1,2,*] Hanna Terletska,[3] C. Moore,[1,2] Chinedu Ekuma,[1,2] Ka-Ming Tam,[1,2] Tom Berlijn,[4,5] Wei Ku,[6,7]
Juana Moreno,[1,2] and Mark Jarrell[1,2]

[1]*Department of Physics and Astronomy, Louisiana State University, Baton Rouge, Louisiana 70803, USA*

[2]*Center for Computation and Technology, Louisiana State University, Baton Rouge, Louisiana 70803, USA*

[3]*Department of Physics, University of Michigan, Ann Arbor, Michigan 48109, USA*

[4]*Center for Nanophase Materials Sciences, Oak Ridge National Laboratory, Oak Ridge, Tennessee 37831, USA*

[5]*Computer Science and Mathematics Division, Oak Ridge National Laboratory, Oak Ridge, Tennessee 37831, USA*

[6]*Condensed Matter Physics and Materials Science Department, Brookhaven National Laboratory, Upton, New York 11973, USA*

[7]*Physics Department, State University of New York, Stony Brook, New York 11790, USA*

We generalize the typical medium dynamical cluster approximation to multiband disordered systems. Using our extended formalism, we perform a systematic study of the nonlocal correlation effects induced by disorder on the density of states and the mobility edge of the three-dimensional two-band Anderson model. We include interband and intraband hopping and an intraband disorder potential. Our results are consistent with those obtained by the transfer matrix and the kernel polynomial methods. We apply the method to $K_xFe_{2-y}Se_2$ with Fe vacancies. Despite the strong vacancy disorder and anisotropy, we find the material is not an Anderson insulator. Our results demonstrate the application of the typical medium dynamical cluster approximation method to study Anderson localization in real materials.

PACS number(s): 71.23.An, 72.80.Ng, 71.10.Fd, 74.70.−b

I. INTRODUCTION

The role of disorder (randomness) in materials has been at the forefront of current research [1–3] due to the new and improved functionalities that can be achieved in materials by carefully controlling the concentration of impurities in the host. At half-filling and in the absence of any spontaneous symmetry breaking field, disorder can induce a transition in a nondegenerate electronic three-dimensional system from a metal to an insulator (MIT) [4,5]. This phenomenon, which occurs due to the multiple scattering of charge carriers off random impurities, is known as Anderson localization [4].

The most commonly used mean-field theory to study disordered systems is the coherent potential approximation (CPA) [6–8], which maps the original disordered lattice to an impurity embedded in an effective medium. The CPA successfully describes some one-particle properties, such as the average density of states (ADOS) in substitutional disordered alloys [6–8]. However, being a single-site approximation, the CPA by construction neglects all disorder-induced nonlocal correlations involving multiple scattering processes. To remedy this, cluster extensions of the CPA such as the dynamical cluster approximation (DCA) [9–11] and the molecular CPA [12] have been developed, where nonlocal effects are incorporated. Unfortunately, all of these methods fail to capture the Anderson localization transition since the ADOS utilized in these approaches is neither critical at the transition nor does it distinguish the extended and the localized states.

In order to describe the Anderson transition in such effective medium theories, a proper order parameter has to be used. As noted by Anderson, the probability distribution of the local density of states (LDOS) must be considered, and the most probable or typical value would characterize it [4,13]. It was found that the geometric mean of the LDOS is a good

approximation of its typical value (TDOS) and it is critical at the transition [14–16], which makes it an appropriate order parameter to describe Anderson localization. Based on this idea, Dobrosavljevic *et al.* [17] formulated a single-site typical medium theory (TMT) for Anderson localization which gives a qualitative description of the transition in three dimensions. In contrast to the CPA, the TMT uses the geometrical averaging over the disorder configuration in the self-consistency loop. And thus, the typical not the average DOS is used as the order parameter. However, due to the single-site nature of the TMT it neglects nonlocal correlations such as the effect of coherent back scattering. Thus, the TMT underestimates the critical disorder strength of the Anderson localization transition and fails to capture the reentrant behavior of the mobility edge (which separates the extended and localized states) for uniform box disorder.

Recently, a cluster extension of TMT was developed, named the typical medium dynamical cluster approximation (TMDCA) [18], which predicts accurate critical disorder strengths and captures the reentrant behavior of the mobility edge. The TMDCA was also extended to include off-diagonal in addition to diagonal disorder. [19]. However, like the TMT, the previous TMDCA implementations have only been developed for single-band systems, and in real materials, there is usually more than one band close to the Fermi level. Sen performed CPA calculation on two-band semiconducting binary alloys [20], and the electronic structure of disordered systems with multiple bands has also been studied numerically in finite systems [21,22]. But a good effective medium theory to study Anderson localization transition in multiband systems is still needed to understand the localization phenomenon in real systems such as diluted doped semiconductors, disordered systems with strong spin-orbital coupling, etc.

In this paper, we extend the TMDCA to multiple band disordered systems with both intraband and interband hopping, and study the effect of intraband disorder potential on electron localization. We perform calculations for both single-site and

_____

*zhangyiphys@gmail.com

finite size clusters, and compare the results with those from numerically exact methods, including transfer matrix method (TMM) and kernel polynomial method (KPM). We show that finite sized clusters are necessary to include the nonlocal effects and produce more accurate results. Since these results show that the method is accurate and systematic, we then apply it to study the iron selenide superconductor $K_x Fe_{2-y} Se_2$ with Fe vacancies, as an example to show that this method can be used to study localization effects in real materials. In addition, as an effective medium theory, our method is also able to treat interactions [23], unlike the TMM and KPM.

The paper is organized as follows. We present the model and describe the details of the formalism in Sec. II. In Sec. III A, we present our results of the ADOS and TDOS for a two-band disordered system with various parameters, and use the vanishing of the TDOS to determine the critical disorder strength, extract the mobility edge, and construct a complete phase diagram in the disorder-energy parameter space for different interband hopping. In Sec. III B, we discuss simulations of $K_x Fe_{2-y} Se_2$ with Fe vacancies. We summarize and discuss future directions in Sec. IV. In the Appendix, we provide justification for the use of our order parameter ansatz.

II. FORMALISM

A. Dynamical cluster approximation for multiband disordered systems

We consider the multiband Anderson model of noninteracting electrons with nearest-neighbor hopping and random on-site potentials. The Hamiltonian is given by

$$
H = -\sum_{\langle ij \rangle} \sum_{\alpha,\beta=1}^{l_b} t_{ij}^{\alpha\beta} (c_{i\alpha}^\dagger c_{j\beta} + c_{j\beta}^\dagger c_{i\alpha})
$$
$$
+ \sum_{i=1}^{N} \sum_{\alpha,\beta=1}^{l_b} (V_i^{\alpha\beta} - \mu\delta_{\alpha\beta}) n_i^{\alpha\beta}. \tag{1}
$$

The first term provides a realistic multiband description of the host valence bands. The labels i,j are site indices and α,β are band indices. The operators $c_{i\alpha}^\dagger$ ($c_{i\alpha}$) create (annihilate) a quasiparticle on site i and band α. The second part denotes the disorder, which is modeled by a local potential $V_i^{\alpha\beta}$ that is randomly distributed according to some specified probability distribution $P(V_i^{\alpha\beta})$, where $n_i^{\alpha\beta} = c_{i\alpha}^\dagger c_{i\beta}$, μ is the chemical potential, and $t_{ij}^{\alpha\beta}$ are the hopping matrix elements. Here we consider binary disorder, where the random on-site potentials $V_i^{\alpha\beta}$ obey independent binary probability distribution functions with the form

$$
P(V_i^{\alpha\beta}) = x\delta(V_i^{\alpha\beta} - V_A^{\alpha\beta}) + (1-x)\delta(V_i^{\alpha\beta} - V_B^{\alpha\beta}). \tag{2}
$$

In our model, there are l_b band indices so that both the hopping and disorder potential are $l_b \times l_b$ matrices. The random potential is

$$
\underline{V_i} = \begin{pmatrix} V_i^{\alpha\alpha} & \cdots & V_i^{\alpha\beta} \\ . & . & . \\ . & . & . \\ . & . & . \\ V_i^{\alpha\alpha} & \cdots & V_i^{\beta\alpha} \end{pmatrix}, \tag{3}
$$

while the hopping matrix is

$$
\underline{t_{ij}} = \begin{pmatrix} t_{ij}^{\alpha\alpha} & \cdots & t_{ij}^{\alpha\beta} \\ . & . & . \\ . & . & . \\ . & . & . \\ t_{ij}^{\beta\alpha} & \cdots & t_{ij}^{\beta\beta} \end{pmatrix}, \tag{4}
$$

where the underbar denotes $l_b \times l_b$ matrix, $t^{\alpha\alpha}$ and $t^{\beta\beta}$ are intraband hoppings, while $t^{\alpha\beta}$ and $t^{\beta\alpha}$ are interband hoppings. Similar definitions apply to the disorder potentials. If we restrict the matrix elements to be real, Hermiticity requires both matrices to be symmetric, i.e., $t^{\alpha\beta} = t^{\beta\alpha}$ and $V_i^{\alpha\beta} = V_i^{\beta\alpha}$.

To solve the Hamiltonian of Eq. (1), we first generalize the standard DCA to a multiband system. Within DCA the original lattice model is mapped onto a cluster of size $N_c = L^3$ with periodic boundary condition embedded in an effective medium. The first Brillouin zone is divided into N_c coarse-grained cells [10], whose center is labeled by K, surrounded by points labeled by $\tilde{k}$ within the cell. Therefore, all the k points are expressed as $k = K + \tilde{k}$. The effective medium is characterized by the hybridization function $\underline{\Delta}(K,\omega)$. The generalization of the DCA to a multiband system entails representing all the quantities in momentum space as $l_b \times l_b$ matrices.

The DCA self-consistency loop starts with an initial guess for the hybridization matrix $\underline{\Delta}(K,\omega)$, which is given by

$$
\underline{\Delta}(K,\omega) = \begin{pmatrix} \Delta^{\alpha\alpha}(K,\omega) & \cdots & \Delta^{\alpha\beta}(K,\omega) \\ . & . & . \\ . & . & . \\ . & . & . \\ \Delta^{\beta\alpha}(K,\omega) & \cdots & \Delta^{\beta\beta}(K,\omega) \end{pmatrix}. \tag{5}
$$

For the disordered system, we must solve the cluster problem in real space. In that regard, for each disorder configuration described by the disorder potential V we calculate the corresponding cluster Green function which is now an $l_b N_c \times l_b N_c$ matrix

$$
\underline{G_c}(V) = (\omega\mathbb{I} - \underline{t}^{(\alpha\beta)} - \underline{\Delta}'^{(\alpha\beta)} - \underline{V}^{\alpha\beta})^{-1}. \tag{6}
$$

Here, $\mathbb{I}$ is identity matrix and Δ'_{ij} is the Fourier transform (FT) of the hybridization, i.e.,

$$
\Delta'^{\alpha\beta}_{ij} = \sum_K \Delta^{\alpha\beta}(K)\exp[iK(r_i - r_j)]. \tag{7}
$$

We then stochastically sample random configurations of the disorder potential V and average over disorder $\langle(\cdots)\rangle$ to get the $l_b N_c \times l_b N_c$ disorder averaged cluster Green's function in real space

$$
\underline{G_c}(\omega)_{ij} = \begin{pmatrix} \langle G_c^{\alpha\alpha}(\omega,V)\rangle_{ij} & \cdots & \langle G_c^{\alpha\beta}(\omega,V)\rangle_{ij} \\ . & . & . \\ . & . & . \\ . & . & . \\ \langle G_c^{\beta\alpha}(\omega,V)\rangle_{ij} & \cdots & \langle G_c^{\beta\beta}(\omega,V)\rangle_{ij} \end{pmatrix}. \tag{8}
$$

We then Fourier transform to K space and also impose translational symmetry to construct the K-dependent disorder averaged cluster Green's function $\underline{G_c}(K,\omega)$, which is a $l_b \times l_b$

matrix for each K component

$$\underline{G_c}(K,\omega) = \begin{pmatrix} G_c^{\alpha\alpha}(K,\omega) & \cdots & G_c^{\alpha\beta}(K,\omega) \\ \cdot & \cdot & \cdot \\ \cdot & \cdot & \cdot \\ \cdot & \cdot & \cdot \\ G_c^{\beta\alpha}(K,\omega) & \cdots & G_c^{\beta\beta}(K,\omega) \end{pmatrix}. \quad (9)$$

After the cluster problem is solved, we can calculate the coarse-grained lattice Green's function matrix

$$\underline{\overline{G}}(K,\omega) = \begin{pmatrix} \overline{G}^{\alpha\alpha}(K,\omega) & \cdots & \overline{G}^{\alpha\beta}(K,\omega) \\ \cdot & \cdot & \cdot \\ \cdot & \cdot & \cdot \\ \cdot & \cdot & \cdot \\ \overline{G}^{\beta\alpha}(K,\omega) & \cdots & \overline{G}^{\beta\beta}(K,\omega) \end{pmatrix}$$
$$= \frac{N_c}{N} \sum_{\tilde{k}} \left[\underline{G_c}(K,\omega)^{-1} + \underline{\Delta}(K,\omega) - \underline{\varepsilon}_k + \underline{\overline{\epsilon}}(K) \right]^{-1}, \quad (10)$$

where the overbar denotes cluster coarse-graining, and $\underline{\overline{\epsilon}}(K)$ is the cluster coarse-graining Fourier transform of the kinetic energy

$$\underline{\overline{\epsilon}}(K) = \underline{E}_0 + \frac{N_c}{N} \sum_{\tilde{k}} \underline{\varepsilon}_k, \quad (11)$$

where $E_0^{\alpha\beta}$ is a local energy, which is used to shift the bands. The diagonal components of Eq. (10) have the same normalization as a conventional, i.e., scalar, Green's function.

The DCA self-consistency condition requires the disorder averaged cluster Green's function equal the coarse-grained lattice Green's function

$$\underline{G_c}(K,\omega) = \underline{\overline{G}}(K,\omega). \quad (12)$$

Then, we close our self-consistency loop by updating the hybridization function matrix using linear mixing

$$\underline{\Delta}_n(K,\omega) = \underline{\Delta}_o(K,\omega) + \xi\left[\underline{G}_c^{-1}(K,\omega) - \underline{\overline{G}}^{-1}(K,\omega)\right], \quad (13)$$

where the subscripts "o" and "n" denote old and new, respectively, and ξ is a linear mixing factor $0 < \xi < 1$. The procedure

above is repeated until the hybridization function matrix converges to the desirable accuracy $\underline{\Delta}_n(K,\omega) = \underline{\Delta}_o(K,\omega)$.

We can see that when the interband hopping, $t^{\alpha\beta}$, and disorder potential, $V^{\alpha\beta}$, vanish all the $l_b \times l_b$ matrices become diagonal, and the formalism reduces to single-band DCA for l_b independent bands.

B. Typical medium theory for multiband disordered systems

To study localization in multiband systems, we generalize the recently developed TMDCA [18] where the TDOS is used as the order parameter of the Anderson localization transition, so the electron localization is captured by the vanishing of the TDOS. We will use this TMDCA formalism to address the question of localization and mobility edge evolution in the multiband model.

Unlike the standard DCA, where the Green's function is averaged over disorder algebraically, the TMDCA calculates the typical (geometrically) averaged cluster density of states in the self-consistency loop as

$$\rho_c^{\text{typ}}(K,\omega) = e^{(1/Nc)\sum_i \langle \log \rho_{ii}(\omega) \rangle} \left\langle \frac{\rho(K,\omega)}{\frac{1}{Nc}\sum_i \rho_{ii}(\omega)} \right\rangle, \quad (14)$$

which is constructed as a product of the geometric average of the local density of states, $\rho_{ii} = -\frac{1}{\pi}\text{Im}G_{ii}(\omega)$, and the linear average of the normalized momentum resolved density of states $\rho(K,\omega) = -\frac{1}{\pi}\text{Im}G_c(K,\omega)$. The cluster-averaged typical Green's function is constructed via the Hilbert transformation

$$G_c^{\text{typ}}(K,\omega) = \int d\omega' \frac{\rho_c^{\text{typ}}(K,\omega')}{\omega - \omega'}. \quad (15)$$

Generalization of the TMDCA to the multiband case is not straightforward since the off-diagonal LDOS $\rho_{ii}^{\alpha\beta}(\omega) = -\frac{1}{\pi}\text{Im}G_{ii}^{\alpha\beta}(\omega)$ is not positive definite. We construct the $l_b \times l_b$ matrix for the typical density of states as

$$\underline{\rho_{\text{typ}}^c}(K,\omega) = \begin{pmatrix} e^{(1/Nc)\sum_i \langle \ln \rho_{ii}^{\alpha\alpha}(\omega) \rangle} \left\langle \frac{\rho^{\alpha\alpha}(K,\omega)}{\frac{1}{Nc}\sum_i \rho_{ii}^{\alpha\alpha}(\omega)} \right\rangle & \cdots & e^{(1/Nc)\sum_i \langle \ln |\rho_{ii}^{\alpha\beta}(\omega)| \rangle} \left\langle \frac{\rho^{\alpha\beta}(K,\omega)}{\frac{1}{Nc}\sum_i |\rho_{ii}^{\alpha\beta}(\omega)|} \right\rangle \\ \cdot & \cdot & \cdot \\ \cdot & \cdot & \cdot \\ \cdot & \cdot & \cdot \\ e^{(1/Nc)\sum_i \langle \ln |\rho_{ii}^{\beta\alpha}(\omega)| \rangle} \left\langle \frac{\rho^{\beta\alpha}(K,\omega)}{\frac{1}{Nc}\sum_i |\rho_{ii}^{\beta\alpha}(\omega)|} \right\rangle & \cdots & e^{(1/Nc)\sum_i \langle \ln \rho_{ii}^{\beta\beta}(\omega) \rangle} \left\langle \frac{\rho^{\beta\beta}(K,\omega)}{\frac{1}{Nc}\sum_i \rho_{ii}^{\beta\beta}(\omega)} \right\rangle \end{pmatrix}. \quad (16)$$

The diagonal part takes the same form as the single-band TMDCA ansatz, and the off-diagonal part takes a similar form but involves the absolute value of the off-diagonal "local" density of states.

We construct the typical cluster Green's function through a Hilbert transformation

$$\underline{G_{\text{typ}}^c}(K,\omega) = \begin{pmatrix} \int d\omega' \frac{\rho_{\text{typ}}^{\alpha\alpha}(K,\omega')}{\omega - \omega'} & \cdots & \int d\omega' \frac{\rho_{\text{typ}}^{\alpha\beta}(K,\omega')}{\omega - \omega'} \\ \cdot & \cdot & \cdot \\ \cdot & \cdot & \cdot \\ \cdot & \cdot & \cdot \\ \int d\omega' \frac{\rho_{\text{typ}}^{\beta\alpha}(K,\omega')}{\omega - \omega'} & \cdots & \int d\omega' \frac{\rho_{\text{typ}}^{\beta\beta}(K,\omega')}{\omega - \omega'} \end{pmatrix}, \quad (17)$$

which plays the same role as $G_c(K, \omega)$ in the DCA loop. Once G_{typ} is calculated from Eq. (17), the self-consistency steps are the same as those in the multiband DCA described in the previous section: we calculate the coarse-grained lattice Green's function using Eq. (10), and use it to update the hybridization function matrix of the effective medium via Eq. (13).

The proposed ansatz Eq. (16) has the following properties. When the interband hopping $t^{\alpha\beta}$ and disorder potential $V^{\alpha\beta}$ vanish, it reduces to single-band TMDCA for l_b independent bands, since all the off-diagonal elements of the Green's functions vanish. When disorder is weak, all the $V^{\alpha\alpha}$ are small so the distribution of the LDOS becomes Gaussian with equal linear and geometric average so it reduces to DCA for a multiband disordered system.

When convergence is achieved, we use the total TDOS $\rho_{\mathrm{typ}}^{\mathrm{tot}}(\omega)$ to determine the mobility edge which is calculated as the trace of the local TDOS matrix

$$\rho_{\mathrm{typ}}^{\mathrm{tot}}(\omega) = \mathrm{Tr}\left[\frac{1}{N_c}\sum_K \underline{\rho_{\mathrm{typ}}(K, \omega)}\right] = \sum_{\forall \alpha = \beta} \rho_{\mathrm{typ}}^{\alpha\beta}(\omega). \quad (18)$$

This construction of the order parameter may not seem very physical as the typical value of the LDOS should serve as the order parameter [4,13], and the LDOS for the multiband system is the sum of the l_b bands in the local site basis $\rho_i^{\mathrm{tot}} = \sum_{\alpha=\beta} \rho_i^{\alpha\beta}(\omega)$. Therefore, the real order parameter should be the typical value of ρ_i^{tot} defined as the geometric average of the total LDOS, $\exp(\frac{1}{N_c}\sum_i \log \rho_i^{\mathrm{tot}})$, which is invariant under local unitary transformations and is not equal to the $\rho_{\mathrm{typ}}^{\mathrm{tot}}$ defined in Eq. (18).

However, Eq. (18) should also be a correct order parameter as long as it vanishes simultaneously with the typical value of ρ_i^{tot}, and we show this in the Appendix. By considering the distribution of the LDOS in each band, the Appendix shows that when localized states mix with extended states the system is still extended, which is consistent with Mott's insight about the mobility edge [24]. Intuitively, this makes sense as when all the distributions of $\rho_i^{\alpha\alpha}$ are critical then the typical values must behave as $|V - V_{ci}|^{\beta_v}$ near the transition, and so their sum must as well. If one is not critical (on the metallic side) then Eq. (18) will not vanish as $|V - V_c|^{\beta_v}$, as expected. We realize that Eq. (18) cannot describe orbital selective transitions, but in our formalism, the TDOS for each orbital is calculated individually. Therefore the formalism can be used to study more general models such as, for example, those that can host orbital selective Mott transitions, which is not the main focus of this paper.

To test our multiband typical medium dynamical cluster approximation formulation, we apply it to the specific case of a two-band model, unless otherwise stated in Sec. III. Throughout the discussion of our results below, we denote α as a and β as b.

III. RESULTS

A. Two-band model

As a specific example, we test the generalized DCA and TMDCA algorithms for a three-dimensional system with two degenerate orbitals (ab) described by Eq. (1). In this case, both the hopping and disorder potential are 2×2 matrices in the band basis given by

$$\underline{t_{ij}} = \underline{t} = \begin{pmatrix} t^{aa} & t^{ab} \\ t^{ba} & t^{bb} \end{pmatrix} \quad (19)$$

and

$$\underline{V_i} = \begin{pmatrix} V_i^{aa} & V_i^{ab} \\ V_i^{ba} & V_i^{bb} \end{pmatrix}, \quad (20)$$

respectively. The intraband hopping is set as $t^{aa} = t^{bb} = 1$, with finite interband hopping t^{ab}. Here, the hopping matrix is defined as dimensionless so that the bare dispersion can be written as $\underline{\varepsilon_k} = \underline{t}\varepsilon_k$ with $\varepsilon_k = -2t[\cos(k_x) + \cos(k_y) + \cos(k_z)]$ in three dimensions. We choose $4t = 1$ to set the units of energy. We consider the two bands orthogonal to each other, where the local interband disorder $V_i^{\alpha\beta}$ vanishes and the randomness comes from the local intraband disorder potential $V_i^{\alpha\alpha}$ that follows independent binary probability distribution functions with equal strength, $V^{aa} = V^{bb}$ and impurity concentration $x = 0.5$. Since the two orbitals are degenerate and the disorder strength for each band is also identical, the calculated average DOS will be the same for each band, so we only plot the quantities for one of the bands in the following results, as it is enough to characterize the properties of the system.

In our formalism, in order to disorder average instead of performing the very expensive enumeration of all disorder configurations, which scales as 2^{2N_c}, we perform a stochastic sampling of configurations which greatly reduces the computational cost [25]. This is so we can study larger systems. For a typical $N_c = 64$ calculation, 500 disorder configurations are enough to produce reliable results and this number decreases with increasing cluster size.

We first compare the ADOS and TDOS at various disorder strengths V^{aa} (V^{bb}), with a fixed interband hopping $t^{ab} = 0.3$, for different cluster sizes N_c in Fig. 1. Here we use cubic clusters and also the so-called Betts clusters [26], which correspond to parallelepipeds with different shapes covering the three-dimensional cubic lattice. Our TMDCA scheme for $N_c = 1$ corresponds to the analog of the TMT for two-band systems, and the ADOS is calculated with the two-band DCA. To show the effects of nonlocal correlations introduced by finite clusters, we present data for both $N_c = 1$ and $N_c > 1$. We can clearly see that the TDOS, which can be viewed as the order parameter of the Anderson localization transition, gets suppressed as the disorder increases. By comparing the width of the extended state region, where the TDOS is finite, we can see that single-site TMT overestimates localization.

From Fig. 1, we see that the results of TMDCA for $N_c = 64$ and $N_c = 216$ are almost on top of each other, showing a quick convergence with the increase of cluster size. To see this more clearly, we plot in Fig. 2 the TDOS at the band center for two different disorder strengths and various cluster sizes. We see that the results for both cases converge quickly with cluster size. Faster convergence (around $N_c = 38$) is reached for the case further away from the critical region ($V^{aa} = V^{bb} = 0.6$) than for the one closer ($V^{aa} = V^{bb} = 0.7$) where convergence is reached around $N_c = 98$. This is expected due to the critical
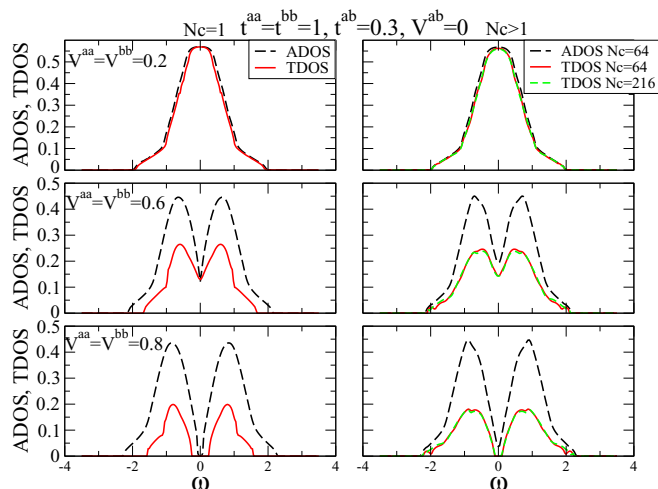
FIG. 1. (Color online) Evolution of the ADOS and TDOS at different disorder strengths V^{aa} (V^{bb}) with the impurity concentration $x = 0.5$, for $N_c = 1$ (left panel) and $N_c > 1$ (right panel) for fixed $t^{ab} = 0.3$. For small disorder, the ADOS and TDOS are almost identical. The TDOS is suppressed as the disorder increases. The extended states region with finite TDOS for $N_c = 1$ is narrower than the results of $N_c > 1$, which indicates that the single-site TMT overemphasizes localization.

slowing down close to the transition. To further study the convergence, we also plot in Fig. 3 the TDOS at the band center as a function of disorder strength ($V^{aa} = V^{bb}$) for several N_c. The critical disorder strength is defined by the vanishing of the TDOS ($\omega = 0$). The results show a systematic increase of the critical disorder strength as N_c increases, and the convergence is reached at $N_c = 98$ with the critical value of 0.74.

To study the effect of interband hopping t^{ab}, we calculate the disorder-energy phase diagram for the case with vanishing
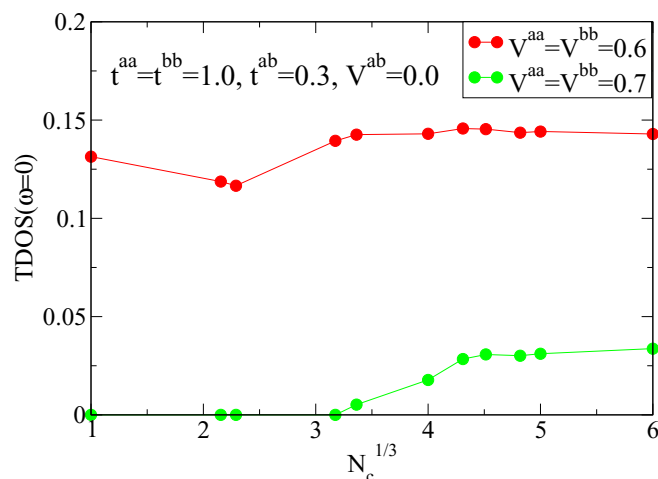
FIG. 2. (Color online) Evolution of the TDOS at the band center ($\omega = 0$) with increasing cluster size for two different sets of parameters with $t^{aa} = t^{bb} = 1.0, t^{ab} = 0.3, V^{ab} = 0.0, V^{aa} = V^{bb} = 0.6, 0.7$ both with the impurity concentration $x = 0.5$. The former has faster convergence (around $N_c = 38$) than the latter (around $N_c = 98$), due to the critical slowing down closer to the transition region.
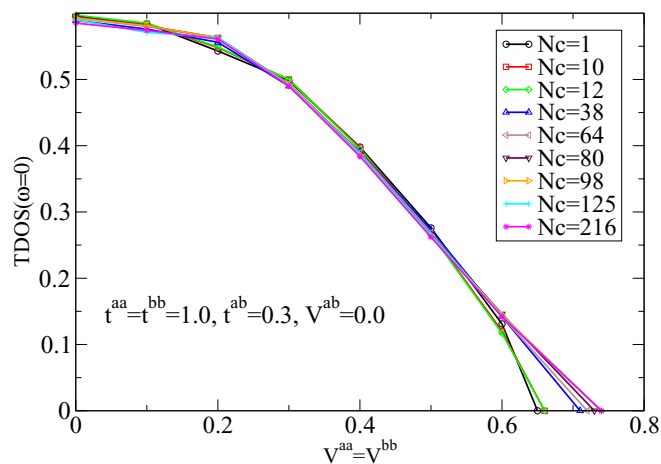

FIG. 3. (Color online) The TDOS at the band center ($\omega = 0$) vs $V^{aa} = V^{bb}$ with increasing cluster size, for $t^{aa} = t^{bb} = 1.0$, $t^{ab} = 0.3$, $V^{ab} = 0.0$. For $N_c = 1$, the critical disorder strength is 0.65 and as N_c increases, it increases and converges to 0.74 for $N_c = 98$.

t^{ab} and finite $t^{ab} = 0.3$ in Fig. 4. The mobility edge is determined by the energy where the TDOS vanishes. By comparing the left and right panels, we can see that introducing a finite t^{ab} makes the system more difficult to localize, causing an upward shift of the mobility edge. The single-site TMT overestimates the localized region compared to finite cluster results. We also compare our results with those from the TMM [27–29] to check the accuracy of the mobility edge calculated from TMDCA. For the TMM, the Schrödinger equation is written in terms of wave-function amplitudes for adjacent layers in a quasi-one-dimensional system, and the correlation (localization) length is computed by accumulating
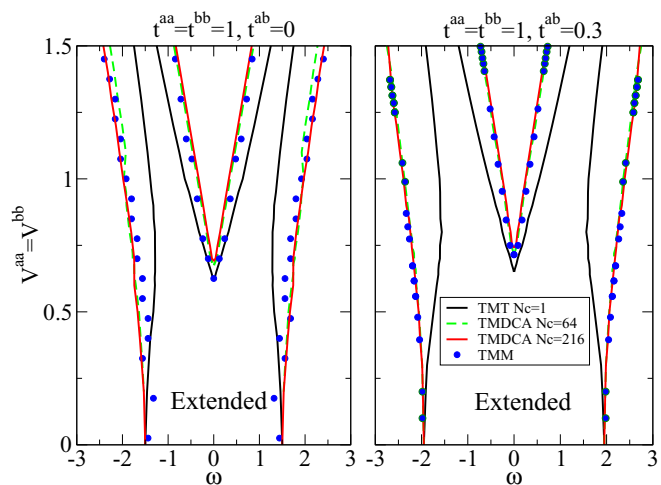

FIG. 4. (Color online) Disorder-energy phase diagram for vanishing t^{ab} (left panel) and finite $t^{ab} = 0.3$ (right panel). We compare the mobility edge obtained from the TMT ($N_c = 1$), TMDCA ($N_c = 64$ and 216), and TMM. Parameters for the TMM data are given in the text (the TMM data for $t_{ab} = 0.0$ is reproduced from [19]). A finite t^{ab} increases the critical disorder strength, indicating that t^{ab} results in a delocalizing effect. The single-site TMT overestimates the localized region.
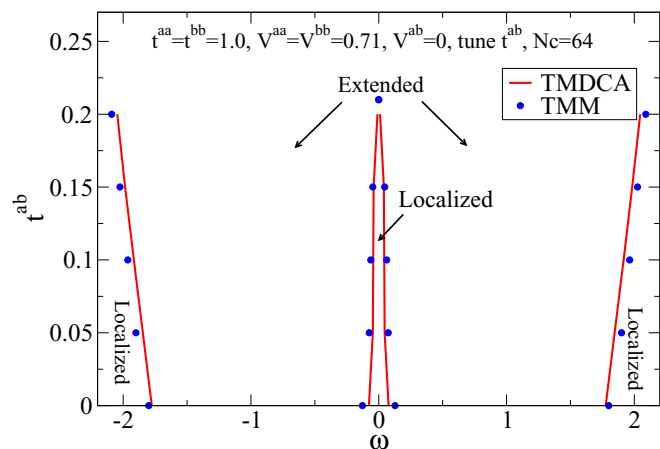
FIG. 5. (Color online) Evolution of the mobility edge as t^{ab} increases, while V^{aa} and V^{bb} are fixed. The results are calculated for $N_c = 64$. A domelike shape shows up around the band center, signaling the closing of the TDOS gap. Parameters for the TMM data are given in the text.
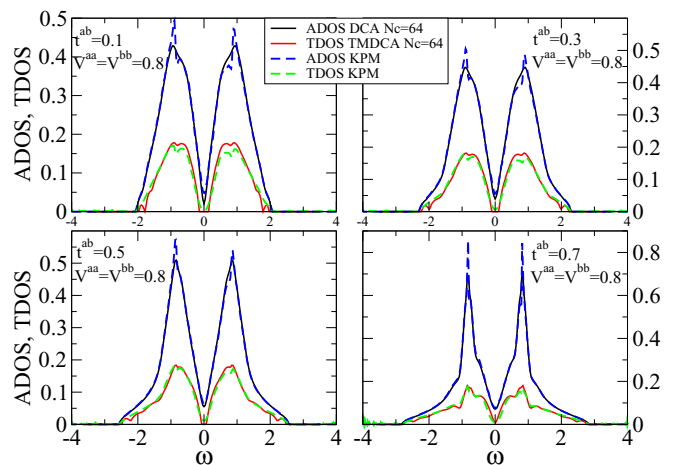

FIG. 6. (Color online) Comparison of ADOS and TDOS calculated with DCA, TMDCA, and KPM with fixed disorder strength $V^{aa} = V^{bb} = 0.8$ with the impurity concentration $x = 0.5$ and various values of interband hopping t^{ab}. The KPM uses 2048 moments on a cubic lattice of size 48^3 and 200 independent realizations generated with 32 sites randomly sampled from each realization.

the Lyapunov exponents of successive transfer matrix multiplications that describe the propagation through the system. All TMM data is for a 3D system of length $L = 10^6$ and the Kramer-MacKinnon scaling parameter $\Lambda(V, M)$ is computed for a given disorder strength V and "bar" width M. The transfer matrix is a $2Ml_b \times 2Ml_b$ matrix. The system widths used were $M = [4\text{–}12]$. The critical point is found by identifying the crossing of the $\Lambda(M)$ vs V curves for different system sizes. The transfer matrix product is reorthogonalized after every five multiplications.

To see the effect of interband hopping more directly, we now consider increasing t^{ab} while keeping the disorder strength fixed ($V^{aa} = V^{bb} = 0.71$), and study the evolution of the mobility edge (Fig. 5). The localized region around the band center starts to shrink as t^{ab} is increased, leading to a small domelike shape with the top located at $t^{ab} = 0.2$. This shows that increasing t^{ab} delocalizes the system, which is reasonable since increasing t^{ab} effectively increases the bare bandwidth.

To further benchmark our algorithms, we plot the ADOS and TDOS calculated with two-band DCA and TMDCA together with those calculated by the KPM [30–33] (Fig. 6). In the KPM analysis, the LDOS is expanded by a series of Chebyshev polynomials, so that the ADOS and TDOS can be evaluated. The details for the implementation of KPM are well discussed in Ref. [31] and the parameters used in the KPM calculations are listed in the caption of Fig. 6. The Jackson kernel is used in the calculations [31]. As shown in the plots, the results from the generalized DCA and TMDCA match nicely with those calculated from the KPM.

The excellent agreement of the TMDCA results with those from more conventional numerical methods, such as KPM and TMM, suggest that the method may be used for the accurate study of real materials.

B. Application to $K_y Fe_{2-x} Se_2$

Next, we demonstrate the method with a case study of Fe vacancies in the Fe-based superconductor $K_x Fe_{2-y} Se_2$, which

has been studied intensely because of its peculiar electronic and structural properties. Early on it was found that there is a strong $\sqrt{5} \times \sqrt{5}$ ordering of Fe vacancies [34]. Later it was discovered that this material also contains a second phase [35,36]. It is commonly speculated that the second phase is the one that hosts the superconducting state and the phase with the $\sqrt{5} \times \sqrt{5}$ vacancy ordering is an antiferromagnetic (AFM) insulator. Recent measurements of the local chemical composition [37,38] have determined that the second phase also contains a large concentration of Fe vacancies (up to 12.5%). However, these Fe vacancies are not well ordered since no strong reconstruction of the Fermi surface [39–41] was observed by angle-resolved photoelectron spectroscopy (ARPES) experiments [42,43].

Interestingly, with such a disordered structure, this material hosts a relatively high superconducting transition temperature of 31 K at ambient pressure [44]. It was the first Fe-based superconductor that was shown from ARPES [42,43] to have a Fermi surface with electron pockets only and no hole pockets, apparently disfavoring the widely discussed $S^{\pm}$ pairing symmetry [45] in the Fe-based superconductors. $K_x Fe_{2-y} Se_2$ is also the only Fe-based superconductor whose parent compound (with perfectly ordered Fe vacancy) is an AFM insulator [46] rather than an AFM bad metal. Furthermore, from neutron scattering [34] it has been observed that the antiferromagnetism has a novel block type structure with a record high Néel temperature of $T_N = 559$ K and magnetic moment of $3.31\mu_B$/Fe. Such a special magnetic structure is obviously not driven from the nesting of the simple Fermi surface, but requires the interplay between local moments and itinerant carriers present in the normal state [47,48].

Given that Fe vacancies are about the strongest possible type of disorder that can exist in Fe-based superconductors and given that the Fe-based superconductors are quasi-two-dimensional materials, it is natural to speculate how close
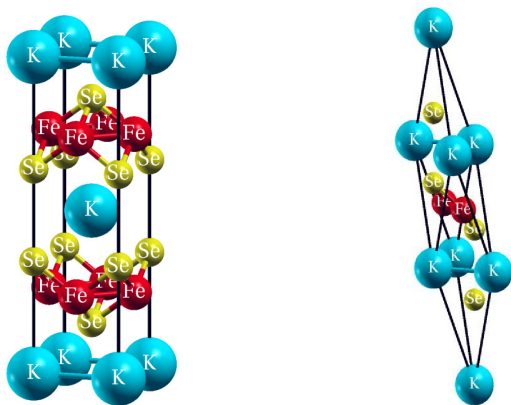
(a) conventional unit cell　　　　(b) primitive unit cell

FIG. 7. (Color online) Crystal structure of KFe_2Se_2.

the second phase is to an Anderson insulator. If it is indeed close, this would have interesting implications for the strong correlation physics and the nonconventional superconductivity in these compounds.

To investigate the possibility of Anderson localization in the second phase of $K_xFe_{2-y}Se_2$ we will employ TMDCA on a realistic first-principles model. To this end we use density functional theory (DFT) in combination with the projected Wannier function technique [49] to extract the low energy effective Hamiltonian of the Fe-d degrees of freedom. Specifically we applied the WIEN2K [50] implementation of the full potential linearized augmented plane wave method in the local density approximation. The k-point mesh was taken to be $10 \times 10 \times 10$ and the basis set size was determined by $RK_{max} = 7$. The lattice parameters of the primitive unit cell [cf. Fig. 7(b)] are taken from Ref. [34]. The subsequent Wannier transformation was defined by projecting the Fe-d characters on the low energy bands within the interval $[-3,2]$ eV. For numerical convenience, we use the conventional unit cell shown in Fig. 7(a) which contains four Fe atoms. Since there are five d orbitals per Fe atom, we are dealing with a 20-band problem. To simulate the effect of Fe vacancies we add a local binary disorder with strength V and Fe vacancy concentration c_a:

$$P(V_i) = c_a \delta(V_i - V) + (1 - c_a)\delta(V_i). \qquad (21)$$

We set the disorder strength to be $V = 20$ eV, much larger than the Fe-d bandwidth, such that it effectively removes the corresponding Fe-d orbitals from the low energy Hilbert space. This will capture the most dominant effect of the Fe vacancies. The Fe concentration is taken to be $c_a = 12.5\%$, which is the maximum value found in the experiments.

Figure 8 presents the ADOS and TDOS, obtained from our multiband TMDCA for which we considered two cluster sizes $N_c = 1$ and $N_c = 2\sqrt{2} \times 2\sqrt{2} \times 2 = 16$. Consistent with the model calculations presented in the previous sections, we find that the TMT ($N_c = 1$) tends to overestimate the localization effects compared to TMDCA results ($N_c = 16$). While the TMT shows localized states within $[0.6, 1.1]$ eV, the TMDCA for $N_c = 16$ finds localized states in the much smaller energy region $[1.0, 1.1]$ eV instead. Apparently a concentration
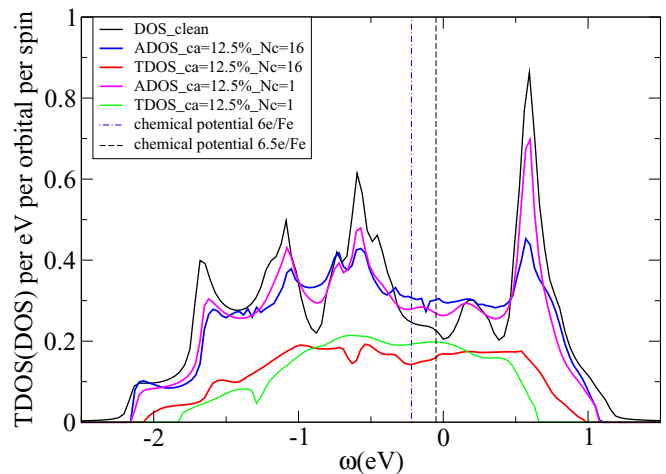

FIG. 8. (Color online) The average and typical density of states of KFe_2Se_2 with 12.5% Fe vacancy concentration calculated by multiband DCA and TMDCA with cluster size $N_c = 1$ and $N_c = 16$, compared with the average density of states of the clean (no vacancy) KFe_2Se_2.

of $c_a = 12.5\%$ is still too small to cause any significant localization effects despite the strong impurity potentials of the Fe vacancies and the material being quasi-two-dimensional. To determine the chemical potential we consider two fillings. The first filling of 6.0 electrons per Fe corresponds to the reported $K_2Fe_7Se_8$ phase [38]. Since strong electron doping has been found in ARPES experiments [42,43], we also consider a filling of 6.5 electrons per Fe. The latter would correspond to the extreme case of no vacancies. Clearly for both fillings the chemical potential remains energetically very far from the mobility edge, and thus far from Anderson insulating.

IV. CONCLUSION

We extend the single-band TMDCA to multiband systems and study electron localization for a two-band model with various hopping and disorder parameters. We benchmark our method by comparing our results with those from other numerical methods (TMM and KPM) and find good agreement. We find that the interband hopping leads to a delocalization effect, since it gradually closes the $\omega = 0$ disorder-induced gap on the TDOS. A direct application of our extended TMDCA could be done for disordered systems with strong spin-orbital coupling. Combined with electronic structure calculations, our method can be used to study the electron localization phenomenon in real materials. To show this, we apply this approach to the iron selenide superconductors $K_xFe_{2-y}Se_2$ with Fe vacancies. By calculating the TDOS around the chemical potential, we conclude that the insulating behavior of its normal state is unlikely due to Anderson localization. This method also has the ability to include interactions [23], and future work will involve real material calculations that fully treat both disorder and interactions.

ACKNOWLEDGMENTS

APPENDIX: THE ORDER PARAMETER DEFINED IN EQ. (18)

We know the system is localized if the distribution of the total LDOS is critical, having a probability distribution $p(\rho_i^{aa} + \rho_i^{bb})$ which is highly skewed with a typical value close to zero. So if we can show that this is true if and only if both ρ_i^{aa} and ρ_i^{bb} are critical, then the critical behavior is basis independent and we can choose any particular basis and use the order parameter defined by Eq. (18) to study the localization transition.

To show this is true, we consider two probability distribution functions $p_1(x_1)$ and $p_2(x_2)$. The probability distribution function for $X = x_1 + x_2$ is

$$P(X) = \int_0^X p_1(x) p_2(X - x) dx, \tag{A1}$$

and we want to show $P(X)$ is critical if and only if both $p_1(x_1)$ and $p_2(x_2)$ are critical.

1. Sufficiency

If both $p_1(x)$ and $p_2(x)$ are critical, then both $p_1(x)$ and $p_2(x)$ are dominated by the region $0 < x < \delta$ where $\delta \to 0^+$. The contribution to the integral in $P(X)$ mainly comes from the region $0 < x < \delta$ and $0 < X - x < \delta$ which is $\max(X - \delta, 0) < x < \min(\delta, X)$. Since δ is infinitesimal, we can assume $X > \delta$, and then we have $X - \delta < x < \delta$. To maximize $P(X)$, we want this region to be as big as possible, so we want $\delta - (X - \delta) = 2\delta - X$ to be as big as possible, which means X must be smaller than $2\delta \to 0^+$. Thus, $P(X)$ is also critical with the typical value around 2δ which is infinitesimal.

2. Necessity

We now consider the case where one of the distributions is not critical. Without loss of generality, we assume $p_2(x)$ is not critical and is peaked at some finite value x_0. We calculate

$$
\begin{aligned}
P(x_0) - P(\delta) &= \int_0^{x_0} p_1(x) p_2(x_0 - x) dx \\
&\quad - \int_0^{\delta} p_1(x) p_2(\delta - x) dx \\
&= \int_0^{\delta} p_1(x)[p_2(x_0 - x) - p_2(\delta - x)] dx \\
&\quad + \int_{\delta}^{x_0} p_1(x) p_2(x_0 - x) dx.
\end{aligned} \tag{A2}
$$

The first term is positive since $p_2(x)$ is peaked around x_0 and $\delta \ll x_0$. The second term is positive obviously, so $P(x_0) > P(\delta)$. Therefore, $P(X)$ is not critical.

In this way we argue that $P(X)$ is critical if and only if both $p_1(x_1)$ and $p_2(x_2)$ are critical. In other words, when the localized states hybridize with extended states, only extended states remain, which is exactly Mott's insight about the mobility edge [24]. The generalization to the multiple band case is trivial.

[1] P. A. Lee and T. V. Ramakrishnan, Rev. Mod. Phys. **57**, 287 (1985).

[2] D. Belitz and T. R. Kirkpatrick, Rev. Mod. Phys. **66**, 261 (1994).

[3] *50 Years of Anderson Localization*, edited by E. Abrahams (World Scientific, Singapore, 2010).

[4] E. Abrahams, P. W. Anderson, D. C. Licciardello, and T. V. Ramakrishnan, Phys. Rev. Lett. **42**, 673 (1979).

[5] B. Kramer and A. MacKinnon, Rep. Prog. Phys. **56**, 1469 (1993).

[6] P. Soven, Phys. Rev. **156**, 809 (1967).

[7] B. Velický, S. Kirkpatrick, and H. Ehrenreich, Phys. Rev. **175**, 747 (1968).

[8] S. Kirkpatrick, B. Velický, and H. Ehrenreich, Phys. Rev. B **1**, 3250 (1970).

[9] M. H. Hettler, M. Mukherjee, M. Jarrell, and H. R. Krishnamurthy, Phys. Rev. B **61**, 12739 (2000).

[10] M. Jarrell and H. R. Krishnamurthy, Phys. Rev. B **63**, 125102 (2001).

[11] M. Jarrell, T. Maier, C. Huscroft, and S. Moukouri, Phys. Rev. B **64**, 195130 (2001).

[12] M. Tsukada, J. Phys. Soc. Jpn. **26**, 684 (1969).

[13] P. W. Anderson, Rev. Mod. Phys. **50**, 191 (1978).

[14] M. Janssen, Phys. Rep. **295**, 1 (1998).

[15] K. Byczuk, W. Hofstetter, and D. Vollhardt, Int. J. Mod. Phys. B **24**, 1727 (2010).

[16] *Log-Normal Distribution—Theory and Applications*, edited by E. Crow and K. Shimizu (Marcel Dekker, NY, 1988).

[17] V. Dobrosavljević, A. A. Pastor, and B. K. Nikolić, Europhys. Lett. **62**, 76 (2003).

[18] C. E. Ekuma, H. Terletska, K.-M. Tam, Z.-Y. Meng, J. Moreno, and M. Jarrell, Phys. Rev. B **89**, 081107 (2014).

[19] H. Terletska, C. E. Ekuma, C. Moore, K.-M. Tam, J. Moreno, and M. Jarrell, Phys. Rev. B **90**, 094208 (2014).

[20] P. N. Sen, Phys. Rev. B **8**, 5613 (1973).

[21] H. Aoki, J. Phys. C **14**, 2771 (1981).

[22] H. Aoki, J. Phys. C **18**, 2109 (1985).

[23] C. E. Ekuma, S.-X. Yang, H. Terletska, K.-M. Tam, N. S. Vidhyadhiraja, J. Moreno, and M. Jarrell, arXiv:1503.00025.

[24] N. Mott, J. Phys. C **20**, 3075 (1987).

[25] C. E. Ekuma, C. Moore, H. Terletska, K.-M. Tam, J. Moreno, M. Jarrell, and N. S. Vidhyadhiraja, Phys. Rev. B **92**, 014209 (2015).

[26] D. D. Betts and G. E. Stewart, Can. J. Phys. **75**, 47 (1997).

[27] P. Markoš, Acta Phys. Slovaca **56**, 561 (2006).

[28] A. MacKinnon and B. Kramer, Z. Phys. B **53**, 1 (1983).

[29] B. Kramer, A. MacKinnon, T. Ohtsuki, and K. Slevin, Int. J. Mod. Phys. B **24**, 1841 (2010).

[30] G. Schubert and H. Fehske, in *Quantum and Semi-classical Percolation and Breakdown in Disordered Solids*, Lecture Notes in Physics Vol. 762, edited by B. K. Chakrabarti, K. K. Bardhan, and A. K. Sen (Springer, Berlin, Heidelberg, 2009), pp. 1–28.

[31] A. Weiße, G. Wellein, A. Alvermann, and H. Fehske, Rev. Mod. Phys. **78**, 275 (2006).

[32] G. Schubert, A. Weiße, and H. Fehske, Phys. Rev. B **71**, 045126 (2005).

[33] G. Schubert and H. Fehske, Phys. Rev. B **77**, 245130 (2008).

[34] B. Wei, H. Qing-Zhen, C. Gen-Fu, M. A. Green, W. Du-Ming, H. Jun-Bao, and Q. Yi-Ming, Chin. Phys. Lett. **28**, 086104 (2011).

[35] A. Ricci, N. Poccia, G. Campi, B. Joseph, G. Arrighetti, L. Barba, M. Reynolds, M. Burghammer, H. Takeya, Y. Mizuguchi, Y. Takano, M. Colapietro, N. L. Saini, and A. Bianconi, Phys. Rev. B **84**, 060511 (2011).

[36] Z. Wang, Y. J. Song, H. L. Shi, Z. W. Wang, Z. Chen, H. F. Tian, G. F. Chen, J. G. Guo, H. X. Yang, and J. Q. Li, Phys. Rev. B **83**, 140505 (2011).

[37] S. Landsgesell, D. Abou-Ras, T. Wolf, D. Alber, and K. Prokeš, Phys. Rev. B **86**, 224502 (2012).

[38] X. Ding, D. Fang, Z. Wang, H. Yang, J. Liu, Q. Deng, G. Ma, C. Meng, Y. Hu, and H.-H. Wen, Nat. Commun. **4**, 1897 (2013).

[39] C.-H. Lin, T. Berlijn, L. Wang, C.-C. Lee, W.-G. Yin, and W. Ku, Phys. Rev. Lett. **107**, 257001 (2011).

[40] T. Berlijn, P. J. Hirschfeld, and W. Ku, Phys. Rev. Lett. **109**, 147003 (2012).

[41] C. Cao and F. Zhang, Phys. Rev. B **87**, 161105 (2013).

[42] F. Chen, M. Xu, Q. Q. Ge, Y. Zhang, Z. R. Ye, L. X. Yang, J. Jiang, B. P. Xie, R. C. Che, M. Zhang, A. F. Wang, X. H. Chen, D. W. Shen, J. P. Hu, and D. L. Feng, Phys. Rev. X **1**, 021020 (2011).

[43] Y. Zhang, L. X. Yang, M. Xu, Z. R. Ye, F. Chen, C. He, H. C. Xu, J. Jiang, B. P. Xie, J. J. Ying, X. F. Wang, X. H. Chen, J. P. Hu, M. Matsunami, S. Kimura, and D. L. Feng, Nat. Mater. **10**, 273 (2011).

[44] J. Guo, S. Jin, G. Wang, S. Wang, K. Zhu, T. Zhou, M. He, and X. Chen, Phys. Rev. B **82**, 180520 (2010).

[45] I. I. Mazin, D. J. Singh, M. D. Johannes, and M. H. Du, Phys. Rev. Lett. **101**, 057003 (2008).

[46] M.-H. Fang, H.-D. Wang, C.-H. Dong, Z.-J. Li, C.-M. Feng, J. Chen, and H. Q. Yuan, Europhys. Lett. **94**, 27009 (2011).

[47] W.-G. Yin, C.-C. Lee, and W. Ku, Phys. Rev. Lett. **105**, 107004 (2010).

[48] Y.-T. Tam, D.-X. Yao, and W. Ku, Phys. Rev. Lett. **115**, 117001 (2015).

[49] W. Ku, H. Rosner, W. E. Pickett, and R. T. Scalettar, Phys. Rev. Lett. **89**, 167204 (2002).

[50] K. Schwarz, P. Blaha, and G. Madsen, Proceedings of the Europhysics Conference on Computational Physics, Computational Modeling and Simulation of Complex Systems [Comput. Phys. Commun. **147**, 71 (2002)].